Rev. Roum. Sci. Techn.– Électrotechn. et Énerg.
Vol. **68**, *4*, pp. 400–405, Bucarest, 2023

COMPACT TWO-PORT ANTENNA WITH PARASITIC NOTCH AND DEFECTIVE GROUND FOR WIRELESS COMMUNICATION

PRAGYA GUPTA[1], MANISHA BHARTI[1], ANUBHAV KUMAR[2]

Keywords: Multiple input multiple output antenna (MIMO); Ultrawideband (UWB); Wireless local area network notch (WLAN); Wearable applications.

This paper presents a compact multiple input multiple output antenna (MIMO) with a wireless local area network (WLAN) notch characteristic for ultra-wideband (UWB) applications. The two modified rectangular radiators share a common ground that provides UWB response. The design is modeled over FR4 material and has an overall compact size of 0.34 λ_0 × 0.24 λ_0 × 0.015 λ_0 mm^3 at the frequency of 2.9 GHz. A tree-shaped decoupling structure with multiple slots in the ground is introduced between the ports to establish good isolation. The open-ended slots in the ground perturb diminish the surface current between two ports and ensure the isolation larger than 20 dB in the entire UWB from 2.9 GHz to 10.2 GHz. An S-shaped parasitic stub is utilized at the backside of the radiating element to implement a band notch characteristic from 5.03 GHz to 5.90 GHz. The proposed antenna is also investigated for wearable applications with a human tissue model showing a small SAR value (less than 1.6 W/kg). The simulated and measured result shows that the designed antenna suits MIMO performance and wearable devices.

1. INTRODUCTION

In the present scenario, wireless communication systems have been developed extensively due to high data rates and huge channel capacity. Ultra-wideband (UWB) communication has recently attracted appreciable attention to realizing the current requirements [1]. Due to the low transmission power, UWB communication spanning 3.1 GHz to 10.6 GHz is widely employed in short-range applications like Wi-Fi and Bluetooth technology with low power and high bandwidth. UWB technology has significant utilization despite its reliability and multipath fading problems [2]. To address the situation, antenna diversity with UWB technology, which utilizes multiple antennas at both ends, known as the multiple input multiple output (MIMO) system, has been proposed. MIMO utilizes the multipath fading problem as a favorable condition [3] compared to single-element antenna [4]. UWB-MIMO system effectively improves transmission efficiency, communication quality, and channel capacity, suppressing multipath fading with the same consumption of bandwidth and power [5].

To design the MIMO antennas for UWB range, compact, high isolation, wide bandwidth with band-notched behavior have drawn widespread attention in the research field. Designing a compact MIMO antenna increases the electromagnetic interaction between closely spaced elements that degrade the antenna performance. Many technologies are employed to reduce mutual coupling by perturbing the surface current between the ports. DGS [6] utilizes different shapes in the ground that affect the surface current and reduce the mutual coupling by increasing the current path. DGS with stubs is also incorporated to diminish the common coupling connecting multiple antenna elements by changing the surface current [7,8]. Parasitic elements and stubs [9–13] compensate for the mutual impedance by suppressing the surface wave.

In contrast, electromagnetic bandgap (EBG) structure [14,15] and metamaterial [16] affect the antenna property due to the surface current. Furthermore, EBG and meta-material increase the antenna size when placed between antenna elements, and shorting pins increase the electric length of the antenna and affect the impedance matching. Multiple EBG structures can be employed to decrease the mutual coupling for UWB frequency, which increases the antenna size, where stubs, shorting pins, and defected ground are suitable for the narrowband application.

In [6], orthogonal polarization and DGS are used to improve the isolation for wireless body area network applications. In [7], DGS and slotted-T decoupling structure is used between two modified fractal Koch radiators to improve the isolation. Two rectangular-shaped radiators are isolated with T-shaped stubs and open-ended slots in the ground [8]. In [9], the isolation of a modified hexagonal-shaped antenna is enhanced using a T-shaped design in the ground. In [10], two simple rectangular-shaped radiators utilize a simple T-shaped stub with defective ground technology to reduce mutual coupling. In [11], the isolation of the monopole antenna is improved by vertical stubs and an H-shaped slot in the bottom layer of the substrate where the vertical stub elongates the current path, and the H-shaped slot concentrates the current around it, improving the isolation. In [12], a rectangular stub is introduced in the ground plane between two circular radiators to enhance the isolation.

In [13], a T-shaped stub is utilized between two hexagonal-shaped radiators to suppress the current from port I to port II. In [14,15], the sequence of EBG structure in the top substrate layer with a T-shaped stub attached to the ground is designed to enhance the isolation. In [16], two orthogonally placed tapered-fed radiators utilize double split ring resonators between the antenna ports to improve the isolation. In [17], meta-material structures and stubs are designed to isolate the two modified circular patches. In [18], two-element tapered fed radiators are designed to obtain the UWB, and a modified T-shaped stub with a Minkowski fractal shape is incorporated between the two elements to enhance the isolation. In [19], the mutual coupling is reduced using two inverted L-shaped stubs and DGS between two cup-shaped radiators. In [20], current flow between leaf-shaped ports is reduced with stubs, parasitic stubs, and shorting pins.

This paper uses a tree-shaped decoupling structure with multiple open slots to enhance the isolation, where an S-shaped parasitic stub in the ground is used to prevent the WLAN band. The isolation in the entire UWB of the designed antenna is greater than 20 dB except for the notch band, which is of a limited size, and the antenna is

[1] Department of Electronics and Communication, [1] National Institute of Technology, Delhi, PINCODE-110040, India
Emails: [1]pragyagupta@nitdelhi.ac.in, [2]manishabharti@nitdelhi.ac.in
[2] Raj Kumar Goel Institute of Technology & Management, Ghaziabad (UP), PINCODE 201003, India, Email: rajput.anubhav@gmail.com

DOI: 10.59277/RRST-EE.2023.68.4.12

evaluated on a human specimen for wearable technology where significant SAR is achieved. The antenna can be used in portable and wearable devices with less complexity and less coupling with the phantom model behind the antenna.

The proposed antenna is designed with simple decoupling technology where the antenna edge-to-edge distance is only 19 mm. The parasitic S-shaped notch completely neglects the WLAN frequency band and can be effectively used in 5G wearable applications.

2. ANTENNA DESIGN

FR4 substrate is considered for designing a compact MIMO antenna with a dielectric constant = 4.4. The geometry of the antenna with overall dimension $0.34\,\lambda_0 \times 0.24\,\lambda_0 \times 0.015\,\lambda_0$ mm^3 at the frequency of 2.9 GHz is represented in Fig. 1a-b, and hardware specimen with top and bottom plane is described in Fig. 1c. The measured parameter of antenna (mm) are as follows: *W*s = 35, *W*1 = 6.5, *W*2 = 1.5, *W*3 = 3.25, *W*4 = 2.25, *W*5 = 7, *W*6 = 2.1, *W*7 = 4, *W*8 = 3, *W*9 = 8.28, *W*10 = 0.5, *W*11 = 2, *W*12 = 2.5, *W*13 = 4, *W*14 = 1, *W*15 = 3.75, *W*16 = 1, *Wf* = 1.5, *W*17=19, *L*5 = 2, *Ls* = 25, *L*4 = 1.5, *L*1 = 8, , *L*3 = 9.5, *L*6 = 10.5, *L*2 = 2 *L*7 = 7, *L*8 = 3, *L*9 = 5, *L*10 = 3.5, *L*11 = 4.5, *L*12 = 3.5, *L*13 = 12.54. The stepwise design methodology of a two-port MIMO antenna with a WLAN notch is displayed in Fig. 2a, and S-parameter characteristics are depicted in Fig. 2b–c. In step 1, two rectangular monopole radiators are accomplished with the partial ground. The ground length is 6.5 mm, and the radiator is 11.5 mm.

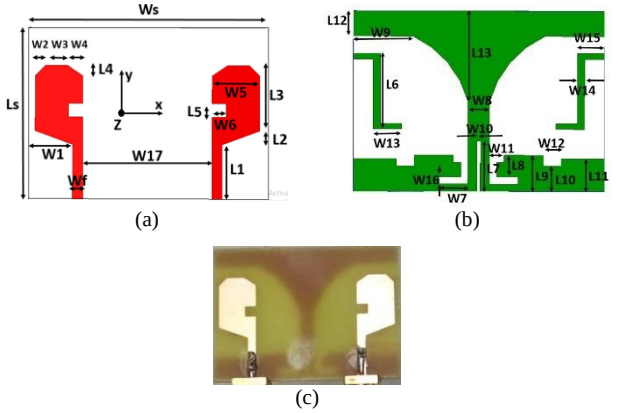

(a) (b)

(c)

Fig. 1 – Two-port proposed antenna: a) front surface; b) back surface; c) hardware prototype.

The $|S_{11}|$ ranges from 3.2 GHz to 9.3 GHz, and minimum $|S_{21}|$ is more than 11.10 dB. In step-2, the rectangular radiator is modified to increase the impedance matching and enhance the impedance bandwidth. The $|S_{11}|$ ranges from 3.3 GHz to 9.9 GHz, whereas $|S_{21}|$ is the same as step-1. In step-3, a tree-shaped stub is incorporated in the ground, which refines the $|S_{11}|$ of the designed antenna and perturbs the current from port I to port II. The tree-shaped decoupling structure improves the isolation and ranges from 13.9 dB to 47.56 dB, where $|S_{11}|$ expands from 3.4 GHz to 9.1 GHz.

Moreover, in step-4, multiple slots in the ground plane mitigate the surface current between the antenna element, which improves the isolation of the antenna and introduces the circular polarization behavior. The isolation of the antenna is above 20 dB and axial ratio (3 dB) bandwidth is from 3.08 GHz to 3.3 GHz. In step-5, a notch characteristic is introduced in the antenna using an S-shaped parasitic stub in the ground. The notch bandwidth is from 5.03 GHz to 5.93 GHz, preventing hiperLAN/1 and hiperLAN/2 in UWB applications. The effect of inserting a tree-shaped decoupling structure and multiple open-ended slots in the ground can also be explained with the current distribution at 7.7 GHz (highest isolation frequency), as shown in Fig. 2d. Introducing a decoupling structure creates an additional path between the radiating elements. The figure shows that the decoupling pattern hinders the current flowing from port I to port II, enhancing the isolation between the ports.

Further, the impact of the S-shaped parasitic stub in the ground to achieve a WLAN notch can be analyzed using surface current in Fig. 2e at 5.2 GHz frequency. The figure shows that the current is concentrated near the parasitic stub, resulting in band notch characteristics from 5 GHz to 5.9 GHz. The L-shaped open stubs in the ground are also responsible for CP behavior from 3.08 GHz to 3.3 GHz, as represented by the 3 dB axial ratio in Fig. 2f. To investigate the CP behavior in-depth, the current distribution at 3.2 GHz frequency at different phases (0^0, 90^0, 180^0, and 270^0) is illustrated in Fig. 2g.

The red arrow indicates the current vector direction. The left side at the ground shows anti-clockwise, and the right side (ground) shows clockwise vector current movement. The clockwise movement represents LHCP behavior, and the anti-clockwise movement represents the RHCP behavior of the proposed antenna. Furthermore, the edge-to-edge distance of the radiator is only 19 mm, which is $0.18\,\lambda_0$ and lower than the conventional distance of $\lambda_0/2$ and $\lambda_0/4$ wavelength, which validates the compactness of the antenna.

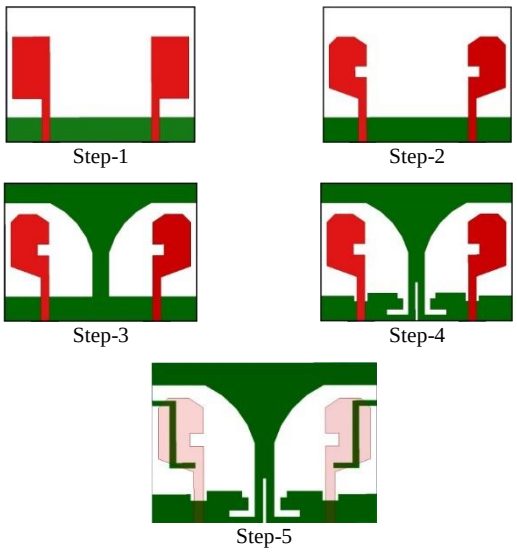

(a)

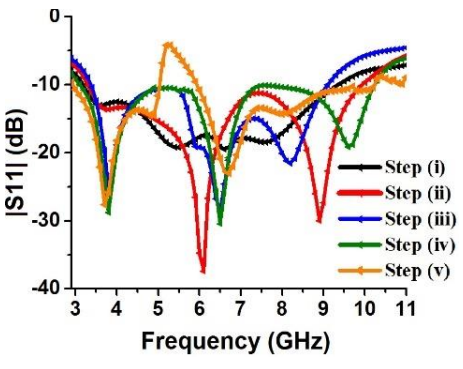

(b)

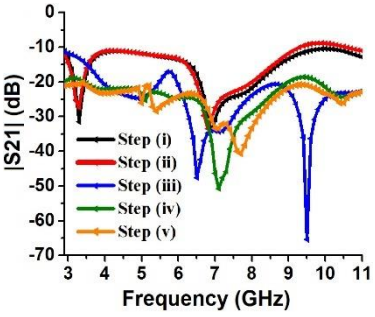

(c)

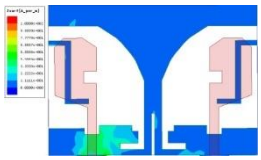

(d)

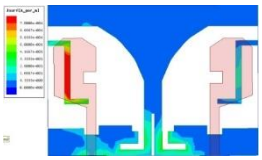

(e)

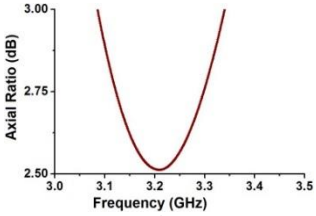

(f)

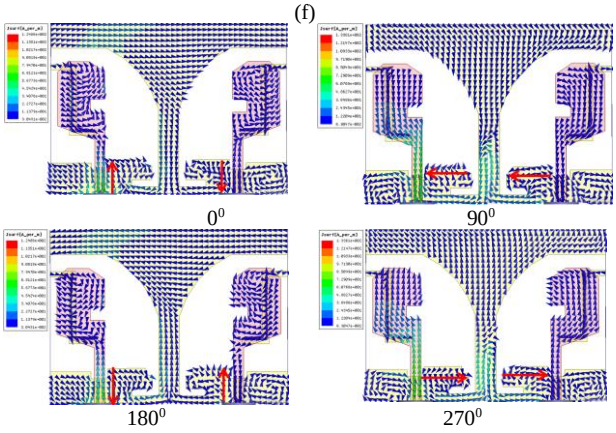

(g)

Fig. 2 – UWB MIMO antenna: a) evolution steps; b) simulated $|S_{11}|$ in dB; c) simulated $|S_{21}|$ in dB; d) current variation at 7.7 GHz; e) current variation at 5.2 GHz; f) axial ratio; g) vector current variation at 3.2 GHz at 0^0, 90^0,180^0, 270^0 phase.

Table 1

Comparison with previous literature

Ref.	Size (mm^2)	Band (GHz)	Isolation (dB)	Decoupling Technique used	Peak Gain(dB)	ECC
6	0.37 λ_0 x 0.37 λ_0	3.1-10.6	-17	Orthogonal polarization and DGS	4.96	0.5
7	0.29 λ_0 x 0.42 λ_0	2.48-15.42	-17	DGS and slotted-T structure	4.75	0.0089
9	0.41 λ_0 x 0.34 λ_0	3.0-10.7	-25	T-shaped metallic strip	5	0.01
10	0.38 λ_0 x 0.29 λ_0	3-11	-20	Rectangular stub and grooves in the ground	5.8	0.02
11	0.28 λ_0 x 0.39 λ_0	3.1-11	-18	H-shaped slot and vertical stub in the ground between the radiator	4.9	0.0005
12	0.3 λ_0 x 0.49 λ_0	3.1-11	-15	Rectangular stub	6.5	0.001
13	0.34 λ_0 x 0.45 λ_0	2.1-11.4	-15	T-shaped stub	0.75	0.04
14	0.29 λ_0 x.0.32 λ_0	3.1-10.6	-20	An array of EBG structure and T-stub	5	0.05
15	0.26 λ_0 x.0.45 λ_0	3-17.6	-18	Array of EBG	4	0.018
17	0.29 λ_0 x.0.58 λ_0	2.6-12	-20	Metamaterial structure	5.5	0.002
Proposed work	0.34 λ_0 x.0.24 λ_0	2.9-10.2	-20	Tree-shaped decoupling structure and multiple open-ended slots	5.37	0.01

3. WEARABLE ANALYSIS

A human wrist model is designed to estimate the effect of electromagnetic waves on the human body. A multilayered human specimen [21] of the size 35 mm × 25 mm comprised of skin (thickness = 2 mm), fat (thickness = 5 mm), and muscles (thickness = 10 mm) is represented in Fig. 3a. The individual properties [22] like dielectric constant (ε_r), mass density (ρ), conductivity (σ), and loss tangent (δ) of the specimen are as follows: skin (ε_r = 36.836 F/m, σ = 2.1474 S/m, ρ = 1109 kg/m^3, δ = 0.283), fat (ε_r= 5.1542 F/m, σ = 0.16627 S/m, ρ = 911 kg/m^3, δ = 0.156) and muscles (ε_r = 51.196 F/m, σ = 2.7358 S/m, ρ = 1090 kg/m^3, δ = 0.259). The model is positioned at a 20 mm distance from the designed antenna. The maximum incident power is taken at 100 mW under the consideration of human safety. According to the FCC specification, the SAR value should not exceed 1.6 W/kg averaged over 1 g of mass. Simulated SAR (local and average) is 0.30 W/kg and 0.13 W/kg, respectively, at a frequency of 3.7 GHz, showing that it is below the permissible value of 1 g of mass. Simulated SAR (local and average) is 0.30 W/kg and 0.13 W/kg, respectively, at a frequency of 3.7 GHz, showing that it is below the permissible value.

The influence of human body specimens on the designed antenna is also examined, and simulated results are expressed in Fig. 3b–d. The S-parameter shows the minimum effect of human specimens on the proposed antenna with the same operating bandwidth except for the lower frequency isolation. The simulated peak realized gain deviated from the expected result. Radiation efficiency is reduced by approximately 10 % from the desired results.

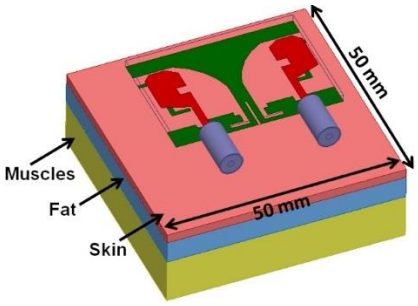

(a)

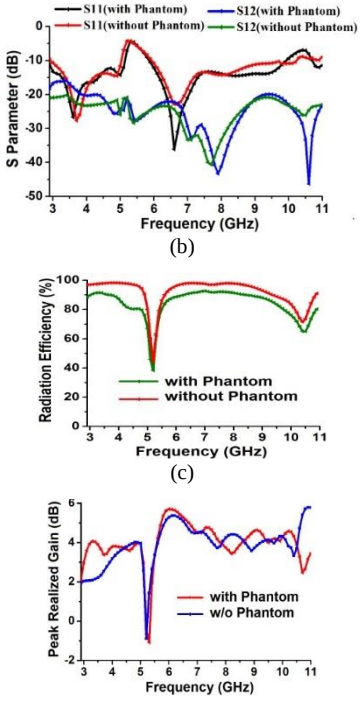

Fig. 3 – a) Human specimen model; b) $|S_{11}|$ and $|S_{21}|$ (dB); c) radiation efficiency; d) Peak gain (dB)

4. RESULTS AND DISCUSSIONS

The FR4 material is utilized to fabricate the two-port UWB MIMO antenna with WLAN notch, simulation is performed on HFSS 13 software, and measurement is carried out on vector analyzer Anritsu MS2038C. Figure 5a represents that the $|S_{11}|/|S_{22}|$ parameter ranges from 2.9 GHz to 10.2 GHz except from 5.0 GHz to 5.9 GHz band notch characteristics, and $|S_{21}|/|S_{12}|$ parameter is more than 20 dB in the desired band. The far-field property is measured in the anechoic chamber at 3.2 GHz, 3.7 GHz, and 6.7 GHz on port I's excitation and port II's termination with the 50-ohm load. The measurement and simulation (normalized) 2D radiation pattern in the *x*-*z* and *y*-*z* planes is represented in Fig. 4b for co and cross-polarization where RHCP and LHCP radiation pattern is achieved at 3.2 GHz. The measured result of the 3 dB axial ratio in Fig. 4c demonstrates the CP behavior from 3.08 GHz to 3.3 GHz. Peak realized gain extends from 1.94 dBi to 5.37 dBi except at the notch frequency, where it drops to a negative value as depicted in Fig. 4d. Radiation efficiency is greater than 90 % in the entire UWB except at the notch, as represented in Fig. 4e. The total efficiency of the MIMO antenna is more than 80 % throughout the band except at the notch, as represented by Fig. 4h. The antenna is designed with proper impedance matching with a 1.5 mm width of microstrip-fed transmission line inspired by half-cut radiator technology. Therefore, fewer deviations are achieved in all the results [23]. The comparative evaluation of the designed antenna is discussed in Table 1, revealing that the proposed antenna is compact in size and higher in bandwidth. It has a lower correlation ratio with a high gain. Therefore, the antenna is suitable for wearable and WLAN applications.

To verify the MIMO performance of the antenna, envelope correlation coefficient (ECC), total active reflective coefficient (TARC), channel capacity loss (CCL), and diversity gain (DG) [24] are calculated and illustrated in Fig. 4i–l. ECC is an essential parameter that represents the correlation between the individual elements of the antenna. The ECC can be measured with the *S*-parameter using

$$\mathrm{ECC}=\frac{\left|S_{11}^{*}S_{12}+S_{21}^{*}S_{22}\right|^{2}}{(1-|S_{11}|^{2}-|S_{21}|^{2})(1-|S_{22}|^{2}-|S_{12}|^{2})}. \quad (1)$$

In literature, the ECC value is considered less than 0.5 for the designed antenna that can be used in practical situations. ECC is less than 0.01 between the ports in the desired band in the designed antenna. TARC of the MIMO antenna can be analyzed using eq. (2) to analyze the performance

$$\mathrm{TARC}=\sqrt{\left|S_{11}+S_{12}e^{j\theta}\right|^{2}+\left|S_{22}+S_{21}e^{j\theta}\right|^{2}}/\sqrt{2}, \quad (2)$$

where θ is the phase difference between the two-port feed. The figure represents the variation of θ from 0^0 to $180^{0,}$ showing that the antenna's bandwidth is less affected by the change in the phase feed difference. CCL is also a significant parameter to define diversity performance. CCL defines capacity loss of channels due to the correlation between the MIMO channels. As the number of channels increases, CCL also increases. It can be calculated using

$$\mathrm{CCL}=-\log_{2}\det(\psi^{R}), \quad (3)$$

where ψ^{R} denotes the correlation matrix, the figure represents that the CCL value is less than 0.4 bits/s/Hz, which shows the acceptable performance of the antenna.

DG is also a considerable parameter that defines the reduction of transmission power after using the diversity technique and can be estimated with the help of the above calculated ECC, utilizing

$$\mathrm{DG}=10\sqrt{1-|\mathrm{ECC}|^{2}}. \quad (4)$$

DG should be approximately 10 dB, which is verified from the figure. All the results are found under an acceptable range and can be used in practical applications.

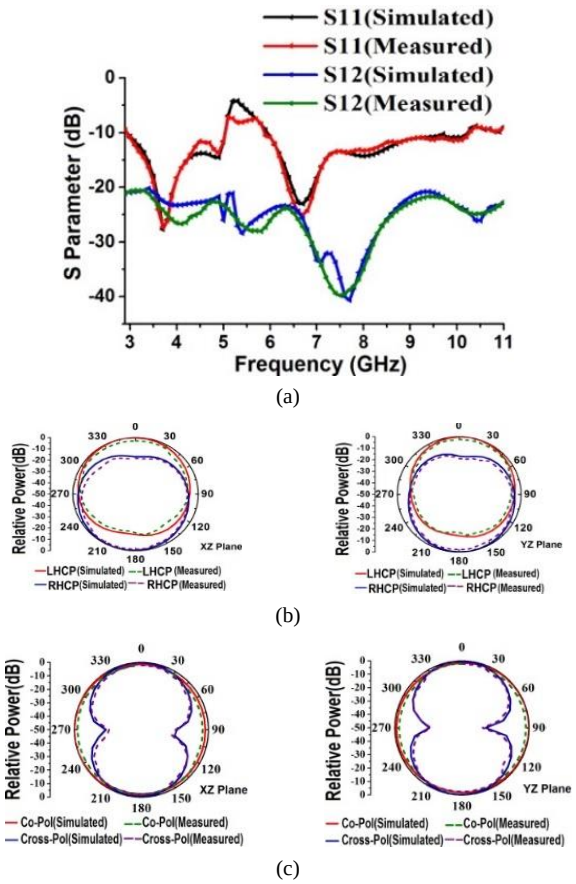

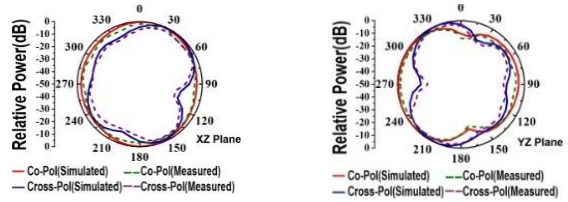

(d)

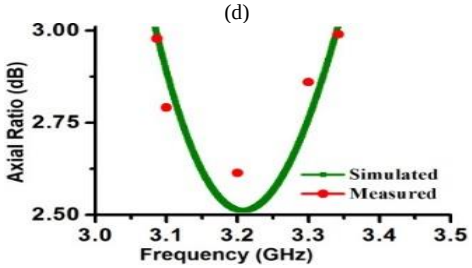

(e)

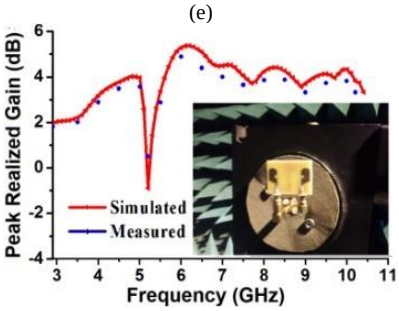

(f)

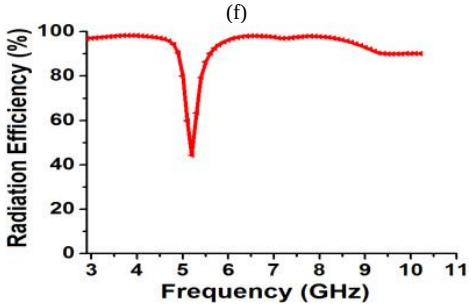

(g)

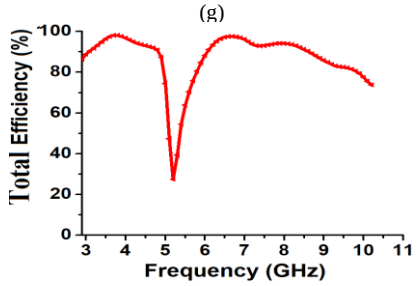

(h)

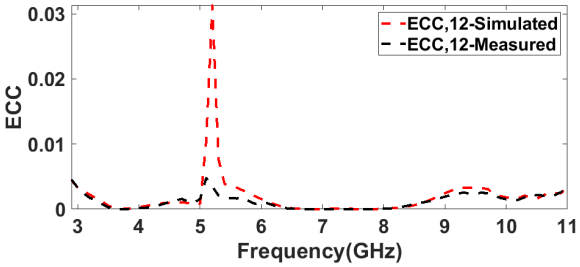

(i)

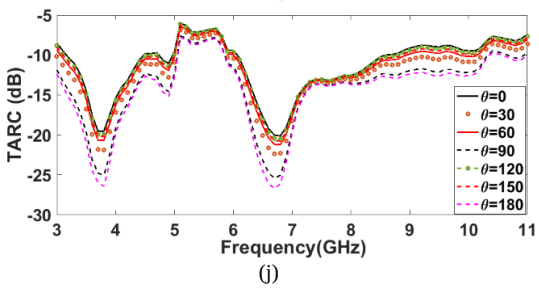

(j)

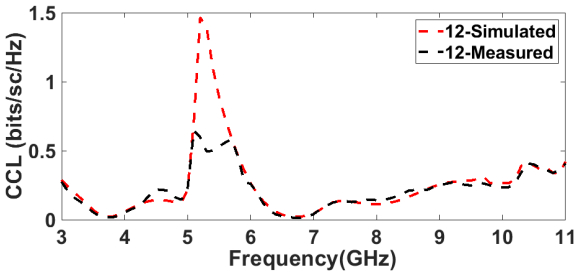

(k)

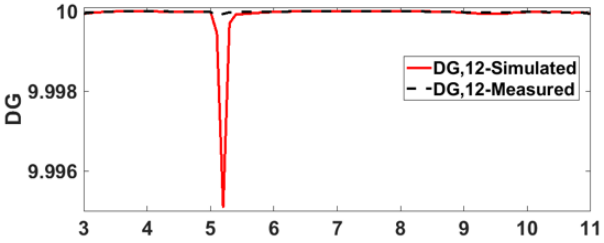

(l)

Fig. 4 – a) Measured S-parameter; radiation pattern b) RHCP and LHCP at 3.2 GHz; c) at 3.7 GHz; d) at 6.7 GHz; e) axial-ratio; f) peak realized gain (dB); g) radiation efficiency (%); h) total efficiency; i) ECC; j) TARC; k) CCL; l) DG.

5. CONCLUSION

The rectangular-shaped two-port UWB antenna with WLAN notch characteristics for wireless and wearable applications is discussed in this paper. The designed antenna covers $|S_{11}|$ from 2.9 GHz to 10.2 GHz with high isolation greater than 20 dB. A tree-shaped decoupling structure with multiple slots in the ground plane is responsible for high isolation in the entire UWB.

An L-shaped parasitic stub backed to a radiating patch is incorporated for WLAN notch characteristics from 5 GHz to 5.9 GHz. The SAR of the designed antenna is less than 1.6 W/kg as the prescribed limit of FCC, which shows that the antenna is suitable for wearable applications.

Received on 5 August 2023

REFERENCES

1. T. Mandal, P. Mandal, P. Mondal, L. Murmu. *Design of dual-band monopole antenna for Bluetooth and ultra-wide band with triple notch using electromagnetic bandgap structure*, Rev. Roum. Sci. Techn. – Électrotechn. et Énerg., **67**, *3*, pp. 307–312 (2022).
2. S. Kareemulla, V. Kumar, *Diversity performance of band notched ultra-wideband MIMO antenna*, Optik, **272**, 170128 (2023).
3. H. Liu, G. Kang, S. Jiang, *Compact dual band-notched UWB multiple-input multiple-output antenna for portable applications*, Microwave and Optical Technology Letters, **62**, *3*, pp.1215–1221 (2020).
4. P. Jha, A. Kumar, N. Sharma, *A metamaterial inspired split ring resonator accomplished multiband antenna for 5G and other wireless applications*, Rev. Roum. Sci. Techn. – Électrotechn. et Énerg., **68**, *2*, pp. 127–131 (2023).
5. P. Pannu, D. K. Sharma, *A low-profile quad-port UWB MIMO antenna using a defected ground structure with dual notch-band behaviour*, International Journal of RF and Microwave Computer-Aided Engineering, **30**, *9*, pp. e22288 (2020).
6. I. Suriya, R. Anbazhagan, *Inverted-A based UWB MIMO antenna with triple-band notch and improved isolation for WBAN applications*, AEU-International Journal of Electronics and Communications, **99**, pp. 25–33 (2019).
7. A.K. Sohi, A. Kaur, *Sextuple band rejection functionality from a compact Koch anti-snowflake fractal UWB-MIMO antenna integrated with split-ring resonators and slots*, AEU-International Journal of Electronics and Communications, **138**, 153898 (2021).
8. P. Gupta, M. Bharti, A. Kumar, *Circular polarized two-element compact dual-band MIMO antenna for 5G and wearable applications*, Rev. Roum. Sci. Techn. – Électrotechn. et Énerg., **67**, *3*, pp. 321–326 (2022).
9. S. Modak, T. Khan. *A slotted UWB-MIMO antenna with quadruple band-notch characteristics using mushroom EBG structure*, AEU-

International Journal of Electronics and Communications, **134**, 153673 (2021).
10. S.D. Luo, Y. Wang, E.L. Chen, C. Jiang, *A compact dual-port UWB-MIMO antenna with quadruple band-notched characteristics*, AEU-International Journal of Electronics and Communications, **136**, 153770 (2021).
11. I.S. Masoodi, I. Ishteyaq, K. Muzaffar, M.I. Magray, *A compact band-notched antenna with high isolation for UWB MIMO applications*, International Journal of microwave and Wireless Technologies, **13**, *6*, pp. 634–640 (2021).
12. B. Premalatha, G. Srikanth, G. Abhilash. *Design and analysis of multi-band notched MIMO antenna for portable UWB applications*, Wireless Personal Communications, **118**, *2*, pp. 1697–1708 (2021).
13. M. Agarwal, J.K. Dhanoa, M.K. Khandelwal, *Two-port hexagon-shaped MIMO microstrip antenna for UWB applications integrated with double stop bands for WiMax and WLAN*, AEU-International Journal of Electronics and Communications, **138**, 153885 (2021).
14. D.Z. Nazif, I.S. Mohamed, A.A. Gaafar, M.A. Abdalla, *UWB notch antennas in MIMO system with high isolation performance*, Radioengineering, **30**, *1* (2021).
15. T. Dabas, D. Gangwar, B.K. Kanaujia, A.K Gautam, *Mutual coupling reduction between elements of UWB MIMO antenna using small size uniplanar EBG exhibiting multiple stopbands*, AEU-International Journal of Electronics and Communications, **93**, pp. 32–38 (2018).
16. C. Sarkar, S. Ray, *Spur line implanted orthogonal microstrip-fed ultra wideband MIMO linear taper slot antenna with WLAN band rejection*, Progress in Electromag. Res. Letters, **101**, pp. 11–17 (2021).
17. A.H. Jabire, A. Ghaffar, A, Li, X.J., Abdu, A., S. Saminu, M. Alibakhshikenari, E. Limiti, *Metamaterial based design of compact UWB/MIMO monopoles antenna with characteristic mode analysis*, Applied Sciences, **11**, *4*, pp. 1542 (2021).
18. A. Bhattacharjee, A. Karmakar, A. Saha, D. Bhattacharya, *Design of a compact UWB MIMO-diversity antenna incorporating fractal inspired isolation structure with band notch characteristics*, Microwave and Optical Technology Letters, **63**, *10*, pp. 2597–2605 (2021).
19. P.K. Patra, M.K. Das, *Modified ground with 50 Ω step fed WLAN notch 2×2 MIMO UWB antenna*, International Journal of RF and Microwave Computer-Aided Engineering, **30**, *3*, pp. e22025 (2020).
20. S.N. Mahmood, A.J. Ishak, A. Jalal, T. Saeidi, S. Shafie, A.C. Soh, Q.H. Abbasi, *A bra monitoring system using a miniaturized wearable ultra-wideband MIMO antenna for breast cancer imaging*, Electronics, **10**, *21*, pp. 2563 (2021).
21. S. Kiani, P. Rezaei, M. Fakhr, *A CPW-fed wearable antenna at ISM band for biomedical and WBAN applications*, Wireless Networks, **27**, pp. 735–745 (2021).
22. http://niremf.ifac.cnr.it/tissprop/htmlclie/htmlclie.php
23. R.N. Tiwari., P. Singh, B.K. Kanaujia, *A half-cut design of low profile UWB planar antenna for DCS/PCS/WLAN applications*, International Journal of RF and Microwave Computer-Aided Engineering, **29**, *9*, pp. e21817 (2019).
24. R. Wu, J. Dong, M. Wang, *Wearable polarization conversion Meta surface MIMO antenna for biomedical applications in 5 GHz WBAN*, Biosensors, **13**, *1*, 73 (2023).